I. Boxx, C. Slabaugh, P. Kutne, R.P. Lucht, W. Meier

3kHz PIV / OH-PLIF measurements in a gas turbine combustor at elevated pressure

3kHz PIV / OH-PLIF measurements in a gas turbine combustor at elevated pressure

Authors: I. Boxx[1], C. Slabaugh[2], P. Kutne[1], R.P. Lucht[2], W. Meier[1]

Affiliations:

[1]   Institut für Verbrennungstechnik
Deutsches Zentrum für Luft- und Raumfahrt (DLR),
D-70569 Stuttgart, DE

[2]   School of Mechanical Engineering
Purdue University
West Lafayette, IN 47907-2088 USA

Corresponding Author:
Dr. Isaac Boxx
Deutsches Zentrum für Luft- und Raumfahrt e.V.
Institut für Verbrennungstechnik
Pfaffenwaldring 38-40
70569 Stuttgart
Germany

Tel. +49-711-6862 732
Fax +49-711-6862 578
isaac.boxx@dlr.de

Colloquium: Diagnostics
Alternate Colloquium: IC Engines

Length of Paper – Based on Method 1

Main Text: 3668 words
      Including Introduction, Body, Conclusions, and Acknowledgments.
References: 385 words
      (20 references + 2) x (2.3 lines/reference) x (7.6 words/line)
Figures:
      Figure 1: $(75 + 10)$mm $\times$ $(2.2$ words/mm$)$ $\times$ $(1$ column$)$ + $(8$ words in caption$)$
          = 195 Words
      Figure 2: $(67 + 10)$mm $\times$ $(2.2$ words/mm$)$ $\times$ $(1$ column$)$ + $(10$ words in caption$)$
          = 179 Words
      Figure 3: $(69 + 10)$mm $\times$ $(2.2$ words/mm$)$ $\times$ $(2$ column$)$ + $(4$ words in caption$)$
          = 352 Words
      Figure 4: $(50 + 10)$mm $\times$ $(2.2$ words/mm$)$ $\times$ $(1$ column$)$ + $(4$ words in caption$)$
          = 136 Words
      Figure 5: $(50 + 10)$mm $\times$ $(2.2$ words/mm$)$ $\times$ $(1$ column$)$ + $(13$ words in caption$)$
          = 145 Words
      Figure 6: $(50 + 10)$mm $\times$ $(2.2$ words/mm$)$ $\times$ $(1$ column$)$ + $(11$ words in caption$)$
          = 143 Words
      Figure 7: $(81 + 10)$mm $\times$ $(2.2$ words/mm$)$ $\times$ $(1$ column$)$ + $(27$ words in caption$)$
          = 227 Words
      Figure 8: $(74 + 10)$mm $\times$ $(2.2$ words/mm$)$ $\times$ $(2$ column$)$ + $(7$ words in caption$)$
          = 377 Words

Total Word Count: 3870+ 385 + 0 + 195 + 179 + 352 + 136 + 145 + 143 + 227 + 377
          = (3970 + 385 + 1754) Words
          = 6011 Words

Abstract

This study was designed to test the feasibility of acquiring simultaneous PIV/OH-PLIF measurements at multi-kHz rates in a turbulent swirl flame at pressures relevant to modern industrial gas turbine combustors. To accomplish this, particle image velocimetry (PIV) and planar laser-induced fluorescence of the hydroxyl radical (OH-PLIF) were applied simultaneously at 3 kHz to study the dynamics of a lean partially-premixed turbulent swirl-stabilized flame of natural gas in an optically accessible, high-pressure combustion test rig at 5 bars. With 0.25mJ/pulse at 283nm for the OH-PLIF measurements, an average signal-to-noise ratio (SNR) of 4.1 was achieved over a region measuring 20×80mm. Absorption of the excitation laser proved to be the greatest challenge in this study, resulting in a significant variation in SNR from one side of the OH-PLIF images to the other. A procedure based on modelling the absorption according to the mean OH-distribution was used to semi-quantitatively correct for this effect. A gradient-based edge-detection algorithm was used to identify reaction zone locations in the resulting images. These were used to compute mean distributions of the flame surface density.

With 2.5mJ/pulse at 532nm for the PIV system, velocity fields measuring 20×80mm were measured at a resolution of 1.25mm. Consistent with prior measurements in the burner, the flame shows strong thermo-acoustic pulsation, with a peak frequency of 388Hz. Phase-averages of the PIV and OH* data indicate these pulsations are driven by the same resonant feedback mechanism responsible for thermo-acoustic pulsation in the burner at atmospheric pressure. No evidence of a precessing vortex core, known to dominate the flow-field of the burner at atmospheric-pressure conditions, was observed.

1. Introduction

The non-intrusive laser imaging diagnostics "particle image velocimetry" (PIV) and "planar laser-induced fluorescence" of combustion radicals, such as hydroxyl (OH-PLIF) or tracers such as toluene or biacetyl (tracer-PLIF), are important tools for studying the dynamics of turbulent flames in gas turbine (GT) combustors. Applied individually, they yield important data on the turbulent flow-field and flame structure. Applied simultaneously, they reveal the interaction of the two. Applied simultaneously and at high (multi-kHz) acquisition rates, they yield critical insight into the flow-flame interactions that drive combustor dynamics and flame stabilization.

Although combustors in modern, large-scale GT power-plants are typically operated at 15-20 bars, the overwhelming majority of simultaneous PIV/PLIF measurements in turbulent swirl flames and (to the authors' knowledge) certainly all those acquired at kHz acquisition-rate have been performed at atmospheric pressure conditions [1-3]. The reason for this is clear. Accomplishing simultaneous PIV/PLIF measurements at elevated pressure is considerably more challenging than at atmospheric pressure conditions.

The use of planar imaging diagnostics at elevated pressure necessitates the use of an optically accessible pressure vessel. Typically, such vessels have multiple windows of thick glass or quartz, which lead to signal degradation from absorption, surface reflections and increased backscatter. The elevated pressure results in pressure-broadening of molecular transitions, beam-steering, and decreased OH mole fractions as a result of increased three-body recombination rates. In addition, it results in increased absorption of the excitation laser compared to atmospheric pressure and increased signal-trapping, wherein the emitted fluorescence is absorbed by other molecules prior to exiting the optically-accessible combustion chamber. The high thermal loads associated with operation at elevated pressure

frequently lead to rapid window fouling and therefore loss of optical access. The use of PIV particles greatly exacerbates this effect.

These considerations make simultaneous PIV/PLIF at elevated pressure particularly challenging even at low repetition-rates, where high-energy (up to several Joules/pulse) pulsed lasers are available. The dominant technology for long-duration (1s or more), kHz-rate OH-PLIF measurements today is the frequency-doubled dye laser pumped with diode-pumped solid state (DPSS) lasers, which typically deliver sub-millijoule pulse-energies. Given the challenges outlined above, it is not clear whether this is sufficient to yield usable OH-PLIF measurements at elevated pressure in an optically-accessible test rig.

The goal of this study was to determine the feasibility of accomplishing simultaneous PIV/OH-PLIF measurements at multi-kHz acquisition rates in a turbulent swirl flame at pressures approaching those found in a modern GT combustor. In addition, this study was designed to identify and characterize the strengths and limitations of this measurement technique by applying it to study the dynamics of a swirl-flame at elevated pressure.

2. Experiment

Figure 1 illustrates the equipment used in this study. The experimental apparatus consists of a swirl burner mounted inside an optically-accessible, high pressure test rig and a set of high acquisition-rate laser imaging diagnostics. Each component is described separately below.

kHz-Rate Diagnostics

The kHz-rate laser diagnostic system (illustrated in Figure 1a) consists of two major components; a PIV system and an OH-PLIF system. Each is described separately below.

PIV System

The PIV system consisted of a dual-cavity diode-pumped, solid-state (DPSS) Nd:YAG laser (Edgewave IS611-DE) and a highspeed CMOS camera (LaVision HSS5). The 532nm wavelength laser was Q-switched to produce 2.6mJ pulse-pairs (temporally separated by $\Delta t = 20\mu s$) at a repetition rate of 3kHz. The laser beam was formed into a 20mm tall planar light sheet using a cylindrical telescope ($f_{PIV1} = -38mm$, $f_{PIV2} = 250mm$) and focused to a waist using a third cylindrical lens ($f_{PIV3} = 700mm$). The flow was seeded with titanium dioxide particles (TiO_2) of $1\mu m$ nominal diameter. Mie scattering from the particles was collected with a 100mm, f/2.8 objective lens (Tokina). A narrowband interference filter (532nm, 3nm FWHM) was used to isolate the scattered signal from background flame luminosity. The 2.6GB onboard memory of the CMOS camera was sufficient to acquire 4096 dual-frame images at 1024×256 pixel resolution per run. The images were de-warped and cross-correlated to extract velocity vectors using a commercial, multi-pass adaptive window offset cross-correlation software package (LaVision DaVis 8). The final interrogation window size and overlap were 16×16 pixels and 50%, respectively. This corresponds to a spatial resolution of 1.25mm and vector spacing of 0.63mm.

OH-PLIF (and OH*) System

The OH-PLIF system consisted of a frequency-doubled dye laser (Sarah Cobra-Stretch HRR) pumped by a Q-switched DPSS laser (Nd:YLF, Edgewave IS-811E) and an intensified, high-framerate CMOS camera (LaVision HSS5 with HS-IRO intensifier). The dye laser used Rhodamine-6G in ethanol and produced approximately 0.25mJ/pulse at 3 kHz. The laser was tuned to 283.2nm (using a laminar reference flame and photomultiplier tube) to excite the isolated Q1(7) line of the A–X (1–0) transition of OH. Laser tuning was checked daily and immediately before measurement runs. The laser pulses were formed into an approximately 20mm tall sheet using a cylindrical telescope ($f_{PLIF1} = -37.5mm$, $f_{PLIF2} = 250mm$) and focused to a thin waist with a third cylindrical lens ($f_{PLIF3} = 1000mm$). The UV laser sheet was

overlapped with that of the PIV system using a 50mm diameter dichroic mirror as shown in Figure 1.

Fluorescence signal was collected at 310nm with a 45mm, f/1.8 objective (Cerco). Elastic scatter (of the 283nm laser) from particles in the flow was blocked using a high transmission (>80% at 310nm) bandpass interference filter (Laser Components GmbH). Background flame luminosity was minimized using a short (100ns) intensifier gate. Spatial non-uniformity of the OH-PLIF excitation sheet was normalized using an ensemble-average image of fluorescence of acetone vapor seeded into the optically-accessible combustion chamber. Spatial variation in camera and intensifier sensitivity was normalized using an ensemble-average image of a uniformly illuminated screen (Kaiser–Slimlite). To match the measurements of the PIV system, 4096 PLIF images were acquired per run at 1024×512 pixel image size, corresponding to a field of view of ≈101×50mm. The images were later cropped to the (≈80×20mm) area illuminated by the PLIF laser sheet. The same camera was used to acquire OH*chemiluminescence image sequences, albeit with longer intensifier gate (5000ns) and without image cropping.

High-Pressure Burner

The burner used in this study is based on the DLR Dual-Swirl Burner (DS-burner). The DS-burner has been extensively characterized at atmospheric pressure conditions and well-described in the literature [4-9]. To date however, it is not well characterized for elevated pressure conditions.

The DS-burner is illustrated in Figure 1b. It consists of an optically-accessible combustion chamber, supplied with fuel and air from a dual-swirl injector. The combustion chamber has a square (80×80mm) cross-section and is 200mm long. It has four large quartz windows for optical access and exhausts through a water-cooled exit plate with a 20mm diameter nozzle designed to isolate the combustion chamber from the surrounding pressure vessel. The dual-

swirl injector consists of a central nozzle (15mm i.d.) mounted coaxially within a concentric, annular nozzle (17mm i.d., 25mm o.d., contoured to an o.d. of 40mm). Radial swirl vanes at the base of each nozzle induce aerodynamic swirl in both nozzles. In the present study, the airstreams are co-swirled. Non-swirling CH_4 is supplied through a ring of 72 square channels (0.5mm×0.5mm) located between the concentric air nozzles. The exit planes of the fuel and central air nozzle are located 4.5mm below the exit plane of the outer air nozzle. A microphone port is located flush with the face of the DS-burner to enable recording of the pressure (thermo-acoustic) fluctuations in the chamber.

The DS-burner is mounted within an optically accessible, high-pressure optical test-rig (DLR-HIPOT). The HIPOT consists of a pressure vessel capable of operation at up to 35 bars pressure, with a thermal load of up to 300kW. The test rig supplies up to 200g/s of combustion air, preheated to 800K. The entire test rig is mounted on a three-axis translation stage, to enable rapid translation of the measurement position without adjustment or realignment of the optical diagnostics system. In the present study, the DS-burner was operated at 5 bars pressure, preheated to 613K. Air and fuel (natural gas) were supplied at rates of 45.2 and 2.11g/s, respectively, to produce a flame with air equivalence ratio $\lambda = 1.3$ and thermal power of ≈ 110kW.

3. Results

The goal of this study was to test the viability of acquiring simultaneous PIV/OH-PLIF measurements at multi-kHz acquisition rates in a swirl flame at elevated pressure using current generation laser and camera technology. The following section therefore focusses primarily upon tests designed to characterize the quality of the measurements.

3.1 - OH-PLIF

Figure 2 shows a representative OH-PLIF image and its corresponding gradient-magnitude. It was acquired in the flame at 5 bars. In this figure, the dark regions (i.e. those with low OH-signal levels) represent gas at low-to-medium temperatures (T < 1500K), e.g. fresh fuel/air mixtures, possibly with some admixture of burned gas. The light-grey regions represent high-temperature (>1500K) combustion products [10]. The brightest areas are associated with regions of super-equilibrium concentrations of OH, mainly generated in the reaction zone of the flame [10]. The mean signal-to-noise ratio (SNR) of the OH-PLIF images acquired in this study is approximately 4.1. The effect of this relatively low SNR is apparent in gradient magnitude image (right) in Figure 2. Whereas the gradients associated with the super-equilibrium OH concentrations associated with the reaction zone are readily apparent in the top half of the image (Y = 0 – 40mm), OH signal gradients in the post-combustion regions of the flow, particularly in the lower half of the image, approach the same magnitude. A key challenge in this study was to robustly identify reaction-zone contours in these low SNR images. The methodology used to accomplish this goal is outlined in Section 3.1.

There is a strong variation in OH-signal from one side of the combustion chamber to the other, resulting in a significant variation in SNR. This clearly results from absorption of the laser sheet by OH in the combustor. Such absorption is frequently observed at elevated pressure conditions [11] and is an unavoidable phenomenon. In the absence of saturation, laser absorption (I/I_0) is independent of the initial intensity. Nonetheless, the low pulse energy of the PLIF excitation laser in this study makes this effect particularly noticeable.

Figure 2 illustrates several important features of the flame. Compared to flames measured in this burner at atmospheric pressure, the reactants show significantly less penetration into the combustor. Consistent with the measurements of [12], the fuel-air mixture appears to have fully reacted within the first 20mm of injector nozzle. In addition, Figure 2 shows considerable penetration of the burned gases into the dual-swirl nozzle. As will be shown

8

later, this results from a strong self-excited thermo-acoustic pulsation in the burner at this run condition.

3.2 - Flame-front extraction

A key parameter of interest in studying turbulence-flame interaction is the spatial location of the reaction zone. As OH persists in post-combustion gases of LPP flames over a time-scale significantly longer than that of the heat-releasing reactions, it is not a direct marker of the flame location. Nonetheless, it is possible (under certain conditions) to extract the reaction zone location from OH-PLIF images. It has been shown [10] that in LPP flames, the reaction zone is identifiable by regions of high OH signal-gradient, due to the super-equilibrium OH concentrations produced there. These high OH-gradient regions also tend to be concentrated along the interface between burned and unburned gas [13,14].

In this study, reaction zones were identified in the PLIF images as shown in Figure 3. First, the raw OH-PLIF image (corrected for camera sensitivity and laser sheet uniformity) was binned (2×2) to improve its SNR, resulting in the image shown in Figure 3a. Inspection of Figure 3a reveals clear indications of laser sheet absorption from one side of the combustion chamber to the other. The dynamic and spatially non-uniform nature of the OH-field in this environment makes shot-by-shot modeling and correction for laser absorption impractical in the present diagnostic configuration. Given the relative continuity of the OH distribution across the chamber observable in Figure 2, modelling laser absorption based on the mean OH-distribution offers a viable (but only semi-quantitative) means of correcting for this effect.

Assuming the OH distribution across the combustor may be approximated by its mean axisymmetric distribution, the laser sheet absorption was modeled according to the Beer-Lambert Law [15],

$$\frac{I}{I_0} = \exp(-\alpha l N) \tag{1}$$

where I_0 and I represent the incident and transmitted beam intensity, respectively, α is the absorption coefficient of the gas, *l* is the path length through the medium and *N* is the number density of absorbing molecules. Based on the ensemble-average of OH-PLIF images, a model for the mean OH distribution across the combustion chamber was computed for each pixel. This modeled OH distribution was used to normalize individual OH-PLIF images, resulting in Figure 3b. Although clearly not a rigorous quantitative correction for individual PLIF images, Figure 3b shows that this model does significantly improve contrast of the OH-PLIF images in a physically plausible fashion and yields some insight into the flame structure where it may otherwise be not available.

Next, the images were locally smoothed with a 5×5 pixel median filter, followed by an edge-preserving, nonlinear diffusion filter (NLD – [16,17]) resulting in the image shown in Figure 3c. Flame-edges were detected using a Gaussian-smoothed Sobel gradient filter, resulting in a gradient magnitude images similar to that shown in Figure 3d. It is clear from Figure 3d that gradients remain in those regions of the image known to consist of burned gas. Prior research on the DS-Burner [7,10] has shown that the majority of reaction zones in this burner are found at the interface of burned and unburned gases. Therefore, the smoothed OH-PLIF images were binarized according to a low, user-defined threshold to create individual image masks corresponding to regions of unburned gas. These masks were used to eliminate gradients beyond a set distance (5 pixels) from a region of unburned gas, resulting in images similar to that shown in Figure 3e. These images were then binarized according to a gradient magnitude threshold and morphologically thinned to single-pixel width contours, shown in Figure 3f. Figure 3g shows the resulting flame-contours, overlaid on the original PLIF images.

Figure 3g illustrates that despite low SNR, the OH-PLIF images yield a physically reasonable (albeit qualitative) representation of the reaction zones present in the OH-PLIF image shown in Figure 2. As a single-frame image may not be representative, the entire OH-

PLIF measurement run was processed according to the steps outlined above. The resulting flame-contour images were then used to compute the mean flame surface density (FSD), shown in Figure 4. Although computed with the modeling assumptions outlined above, the approximately symmetric, V-shaped profile of the FSD contours is consistent with prior work on the DS-burner, suggesting the image processing routine is accurate capturing the majority of reaction zones in the images.

3.3 – Velocity Data

Figure 5 shows a raw, unfiltered velocity field measurement acquired with the PIV system at 5 bars. For the sake of clarity, every third velocity vector is plotted. The background contours represent axial velocity. This measurement was acquired simultaneously with the OH-PLIF image from Figure 2 and shows also the reaction zone identified in Figure 3.

Figure 5 demonstrates the result of a number of design trade-offs that were necessary to implement the kHz-PIV system in this experiment. The first of these was vector resolution vs. SNR. Spatial resolution of 1.25mm was achieved by processing the PIV images to 16×16 pixel interrogation box sizes, resulting in a noisier vector field than would have been achievable with a larger window. The spatial resolution was, in turn, restricted by the goal of measuring the entire chamber-width in a single image. Figure 5 shows the PIV system performed poorly in the vicinity of windows, particularly the lower one, where strong reflections of the 532nm laser resulted in frequent image saturation and poor particle cross-correlations in that area.

Consistent with prior measurements taken in the same burner [12], a strong reverse flow is observed in Figure 5 in the vicinity of the injector nozzle. Away from the nozzle, the flow is observed to travel almost parallel to the burner face toward the window, indicating the inner recirculation zone has a very wide opening angle. The location of the reaction zone in this image is consistent with the velocity field. In the vicinity of the injector nozzle, where strong

reverse flow exists, the flame is quite flat and aligned parallel to the burner face. Away from the injector, where the velocity field indicates greater penetration of unburned reactants into the combustor, the reaction zone is more wrinkled and away from the injector face.

4 – Flame Dynamics

Although a detailed exploration of the dynamics of the DS-burner is beyond the scope of this study, it is instructive to apply a number of standard analysis techniques to the measurement data and compare the results to prior measurements in the similar flames.

4.1 - Frequency Spectra

Figure 6 shows the mean axial velocity field computed from the ensemble-average of all PIV images acquired in the flame during a single imaging run. Prior measurements in the DS-burner at atmospheric pressure [4,5] have shown its flow-field is dominated by a strong inner recirculation zone (IRZ), a conical inflow region and a small outer recirculation zone (ORZ) between the nozzle and the combustion chamber. Similar features are visible in Figure 6, but with a much wider opening angle at the inflow region and stronger reverse flow than is typically seen at atmospheric pressure. The wider opening angle is consistent with chemiluminescence measurements reported in [12], which show a flatter mean flame zone than typically seen at atmospheric pressure. As will be shown later (in Figure 8), this flatter mean flame zone results from a strong axial pulsation of the flow-field disrupting the stable, conical flame-brush generated by this burner at atmospheric pressure.

Figure 6 shows mean axial velocities of up to 25m/s. At this velocity, the fluid will travel ≈ 8.3mm per frame at 3kHz. Given the ≈ 25mm PIV sheet-height, robust tracking of turbulent flow structures from one frame to the next was not possible. The acoustic probe measurements, however, show a strong thermo-acoustic pulsation at ≈ 388Hz, which is well

within the frequency range measured with the PIV system. Given the strong link between thermo-acoustic pulsation and axial velocity fluctuations [18], this frequency should be readily apparent in the velocity field data.

Time-series of axial velocity were extracted at each of the three monitor point locations shown in Figure 6, which correspond to the IRZ, the reactant-inflow region and the shear-layer between the two. The power spectral density (PSD) of axial velocity at each location is plotted in Figure 7, together with that of the acoustic signal. The dominant peak in each is clearly observable at 388Hz, i.e. the thermo-acoustic pulsation frequency. In contrast with measurements acquired at atmospheric pressure in the same burner [8], the spectra do not show the secondary peaks characteristic of a precessing vortex core (PVC). That the PSDs of axial velocity clearly capture the thermo-acoustic pulsation is a good indication of the robustness of the PIV measurements.

It was been shown in [9] that the FSD of flames in this burner fluctuates at approximately the thermo-acoustic frequency. Figure 7e shows the PSD of flame length measured in one of the OH-PLIF image sequences acquired in this study. As expected, it shows a clear peak at the dominant thermo-acoustic frequency (388Hz), suggesting the OH-PLIF measurements provide a reasonable measure of FSD in the combustor, despite strong beam absorption across the combustor.

4.2 – Phase-Averaged Measurements

Figure 8 shows the PIV and OH* chemiluminescence data phase-averaged with respect to the dominant, 388Hz (thermo-acoustic) pulsation, with Phase 1 representing the positive-to-negative zero-crossing of the cycle. OH* is a combustion radical produced in the reaction-zone and acts as a qualitative marker of local heat-release [19,20].

It is clear from Figure 8 that the thermo-acoustic pulsation correlates with a strong variation in flame shape and axial velocity field. From the OH* data, we see the flame

transitions from a relatively compact region of intense heat-release at the burner face at Phase 1-2 to a diffuse, less intense region that fills the entire image by Phase 6-7 and begins to contract again by Phase 8. At Phase 1 the axial velocity field shows a roughly V-shaped IRZ and considerable inflow along the burner face. The previously mentioned effect of laser-reflections is apparent in the noisy mean axial velocity fields at the upper and lower windows. The IRZ expands and strengthens over the acoustic cycle, reaching a peak at Phase 3-4, before weakening and returning to its initial profile. Consistent with phase-averaged measurements acquired at atmospheric-pressure in the same burner [4,5], heat-release peaks during the phase of strongest recirculation, i.e. during Phase 2-3.

Taken together, the data in Figure 8 are consistent with the feedback mechanism suggested in [6], wherein phase-dependent mixing of hot combustion products from the recirculation zone with incoming reactants drives fluctuations in the heat-release rate. The pressure fluctuations this induces lead to strong pulsations in axial velocity.

Summary

Particle image velocimetry (PIV) and planar laser-induced fluorescence of the hydroxyl radical (OH-PLIF) were applied simultaneously at 3 kHz to study the dynamics of a turbulent, swirl-stabilized flame of natural gas in an optically accessible, high-pressure combustion test rig at 5 bars. With 0.25mJ/pulse at 283nm for the OH-PLIF measurements, a mean signal-to-noise ratio of 4.1 was achieved over a region measuring 20×80mm. Absorption of the excitation laser proved to be the greatest challenge in this study, resulting in a significant variation in SNR from one side of the image to the other. A procedure based on modelling the absorption according to the mean OH-distribution was used to semi-quantitatively correct for this effect. A gradient-based edge-detection algorithm was used to identify reaction zone locations in the resulting images. These were used to compute mean distributions of flame surface density.

With 2.5mJ/pulse at 532nm for the PIV system, velocity fields measuring 20×80mm were measured at a resolution of 1.25mm. Consistent with prior measurements in the burner, the flame shows strong thermo-acoustic pulsation, with a peak frequency of 388Hz. Phase-averages of the PIV and OH* data indicate these pulsations are driven by the same resonant feedback mechanism responsible for thermo-acoustic pulsation in the burner at atmospheric pressure. No evidence of a precessing vortex core, known to dominate the flow-field of the burner at atmospheric-pressure conditions, was observed.

The present study demonstrates two key strengths of kHz acquisition-rate PIV / PLIF / OH* chemiluminescence imaging diagnostics in high pressure combustors. These diagnostics enable the non-intrusive measurement of frequency spectra for parameters such as velocity and heat-release throughout the combustor. In addition, the dramatically increased bandwidth of kHz-rate diagnostics enables the acquisition of statistically converged data sets in just seconds, rather than minutes or hours required with conventional 10Hz measurements. This both minimizes costs in expensive high pressure test facilities, but also eliminates the problem of window fouling that has plagued planar laser imaging experiments for many years. The key weakness of these diagnostics is the relatively low SNR of the PLIF imaging system, which makes identification of reaction zones in the flame challenging. This weakness, however, is sure to become less significant as higher pulse-energy kHz-rate laser technology becomes available.

References

1. V. Sick, Proc. Combust. Inst. 34 (2013) 3509–3530

2. B. Böhm, C. Heeger, R. Gordon, A. Dreizler, Flow Turb. Combust. 86 (2011) 313-341.

3. B. Thurow, N.B. Jiang, W.C. Lempert, Meas. Sci. Technol. 24 (2013) 012002.

4. R. Giezendanner-Thoben, U. Meier, W. Meier, M. Aigner. Flow Turbul. Combust. 75 (2005a) 317–333.

5. R. Giezendanner-Thoben, U. Meier, W. Meier, J. Heinze, M. Aigner, Appl. Opt. 44 (2005b) 6565–6577.

6. P. Weigand, W. Meier, X.R. Duan, R. Giezendanner-Thoben, U. Meier, Flow Turbul. Combust. 75 (2005) 275–292.

7. W. Meier, X.R. Duan, P. Weigand, Proc. Combust. Inst. 30 (2005) 825–842.

8. I. Boxx, M. Stöhr, C.D. Carter, W. Meier.Combust. Flame. 157 (2010) 1510–1525

9. A.M. Steinberg, I. Boxx, M. Stöhr, C.D. Carter, W. Meier. Combust. Flame. 157 (2010) 2250–2266.

10. R. Sadanandan, M. Stöhr, W. Meier, Appl. Phys. B 90 (2008) 609–618.

11. P.A. Strakey, S.D. Woodruff, T.C. Williams, R.W. Schefer, AIAA J. 46 (2008) 1604–1613.

12. B.K. Kapadia, P. Kutne, I. Boxx, J. D. Gounder, W. Meier, M. Aigner. Paper P4-28. Proceedings. 6th European Combustion Meeting (ECM), 25.-28.06.2013, Lund, Sweden.

13. M. Sweeney, S. Hochgreb. Appl. Optics. 48:19 (2009) 3866 – 3877.

14. A. E. Bayley, Y. Hardalupas, A. M. K. P. Taylor. Exp. Fluids. 52:4 (2012) 963-983.

15. A. Eckbreth. Laser Diagnostics for Combustion Temperature and Species, Second Edition. Combustion Science and Technology Book Series, Volume 3. Gordon and Breach Publishers. (1996)

16. P. Perona, J. Malik. IEEE Trans. Pattern Anal. Mach. Intell., 12:7 (1990) 629 – 639.

17. J. Weickert, B.M.T.H. Romeny, M.A. Viergever. IEEE Trans. Image Process. 7:3, (1998) 398–410.

18. T. Lieuwen, V. Yang. Combustion Instabilities in Gas Turbine Engines: Operational Experience, Fundamental Mechanisms, and Modeling, AIAA, (2005).

19. N. Docquier, S. Candel. Prog Energy Combust Sci 28 (2002) 107–150.

20. Y. Hardalupas, M. Orain. Combust Flame. 139 (2004) 188–207.
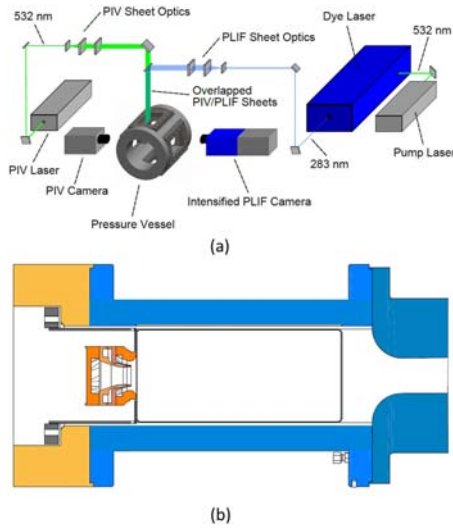
Figures

Figure 1 – Experimental setup. a) Laser diagnostics and test rig b) DS-burner
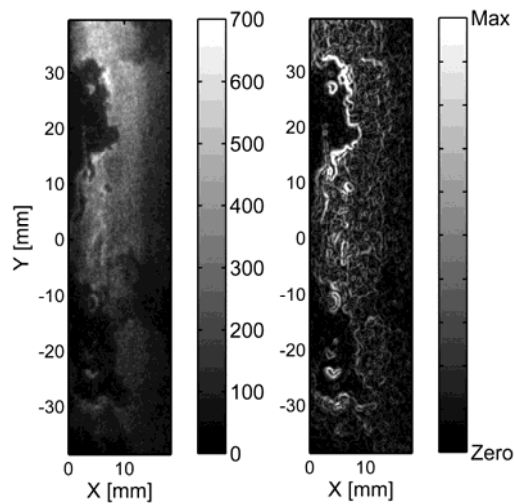

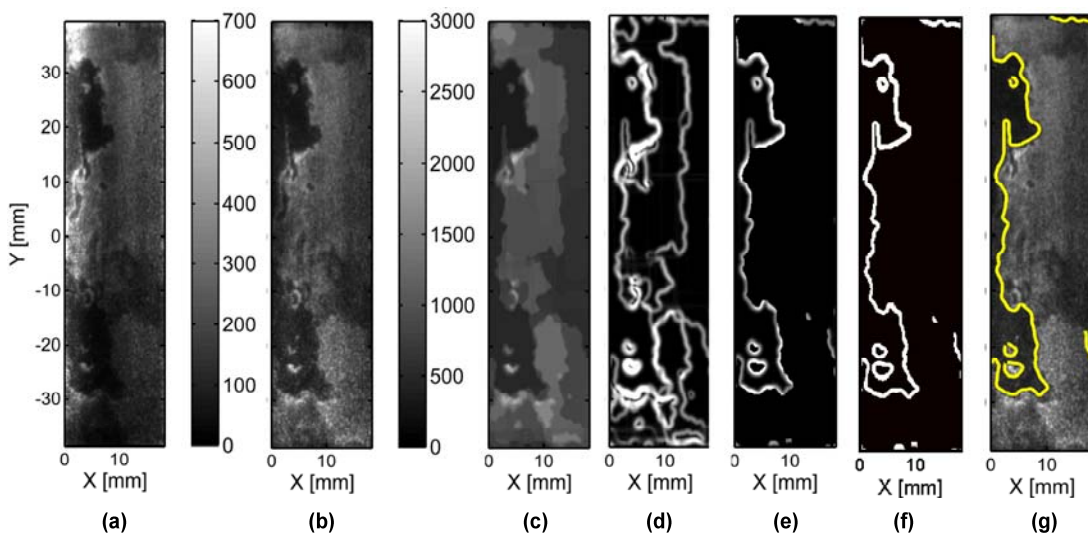Figure 2 – Sample OH-PLIF image. Laser sheet propagates from top to bottom.

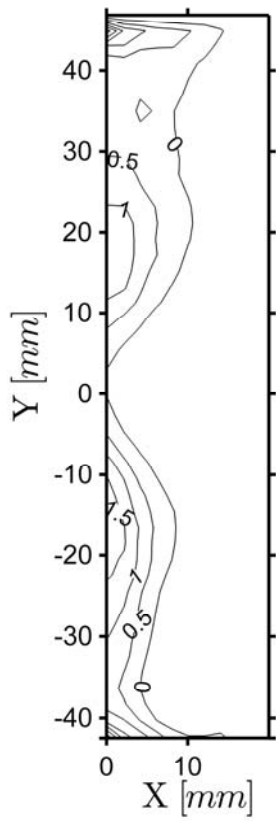Figure 3 – Flame front extraction routine.
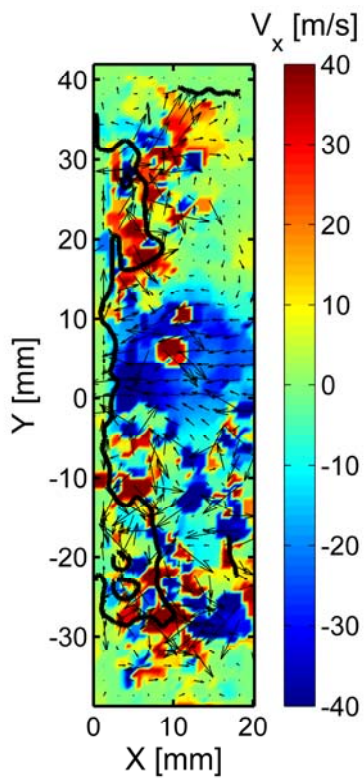
17

Figure 4 – Mean flame surface density.

Figure 5 – Sample PIV measurement and the reaction zone identified in the corresponding OH-PLIF image.
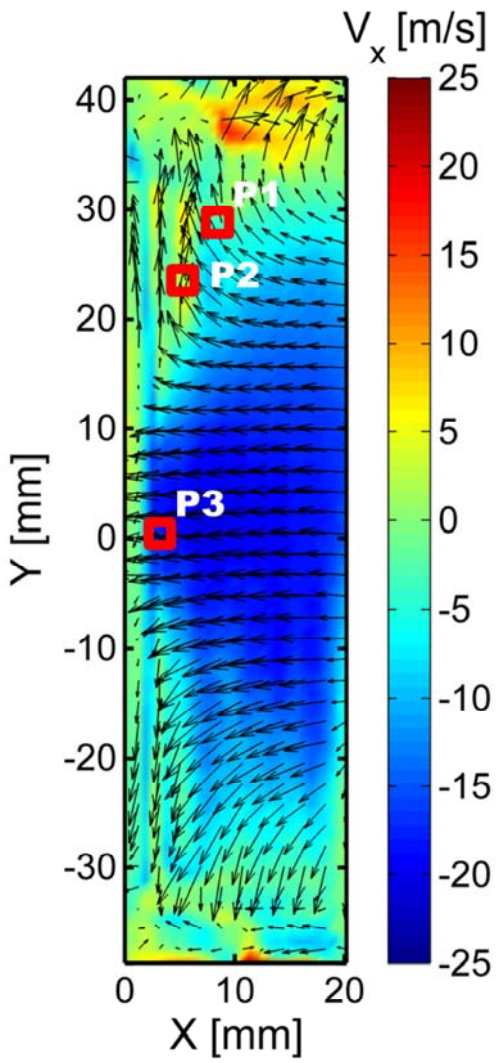
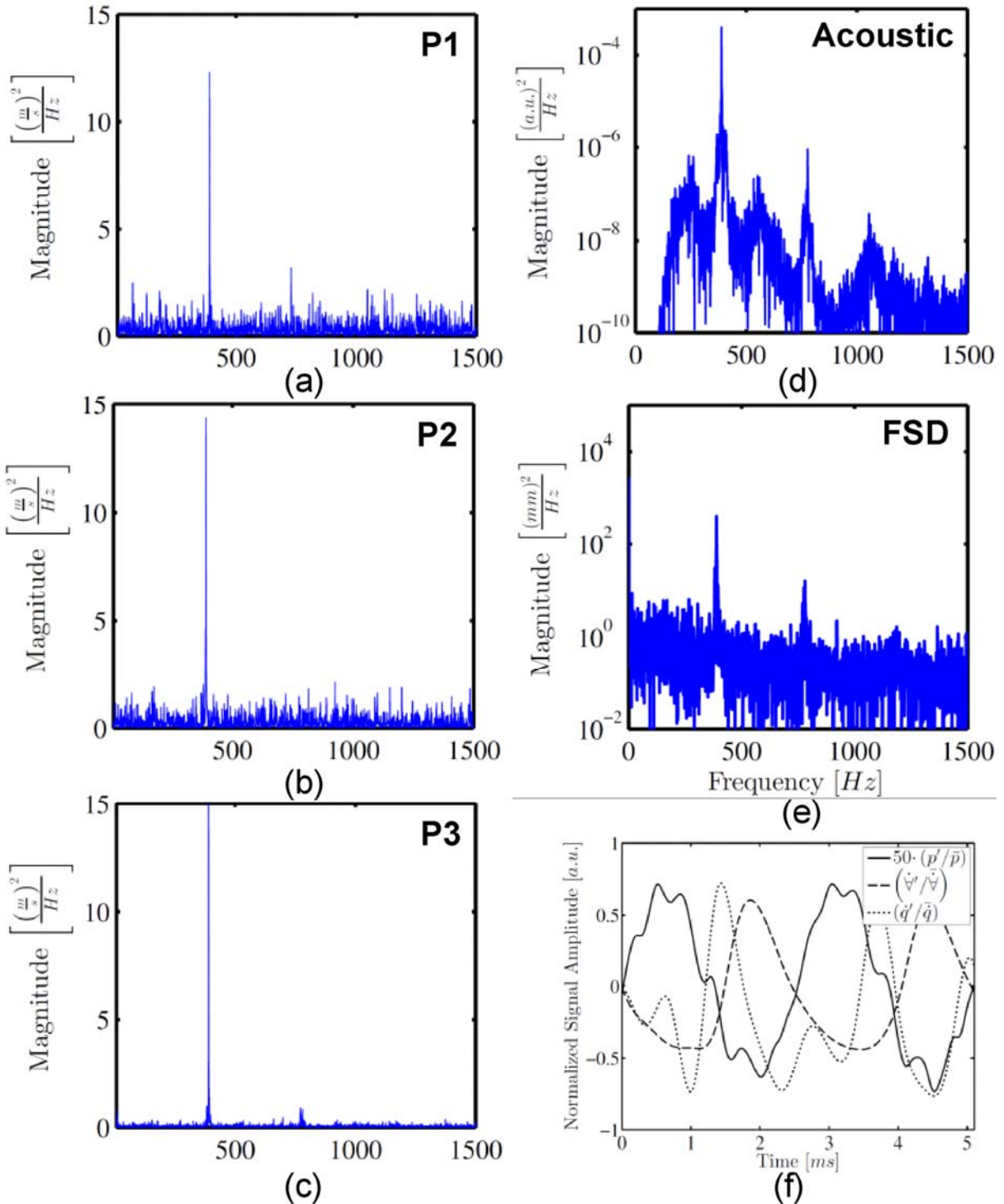Figure 6 – Mean axial velocity field and monitor points where PSDs were computed.

Figure 7 – Power spectral density of a) axial velocity at P1, b) axial velocity at P2, c) axial velocity at P3, d) acoustic signal, e) total flame-length. f) Trace of pressure, flow-rate and heat-release fluctuations.
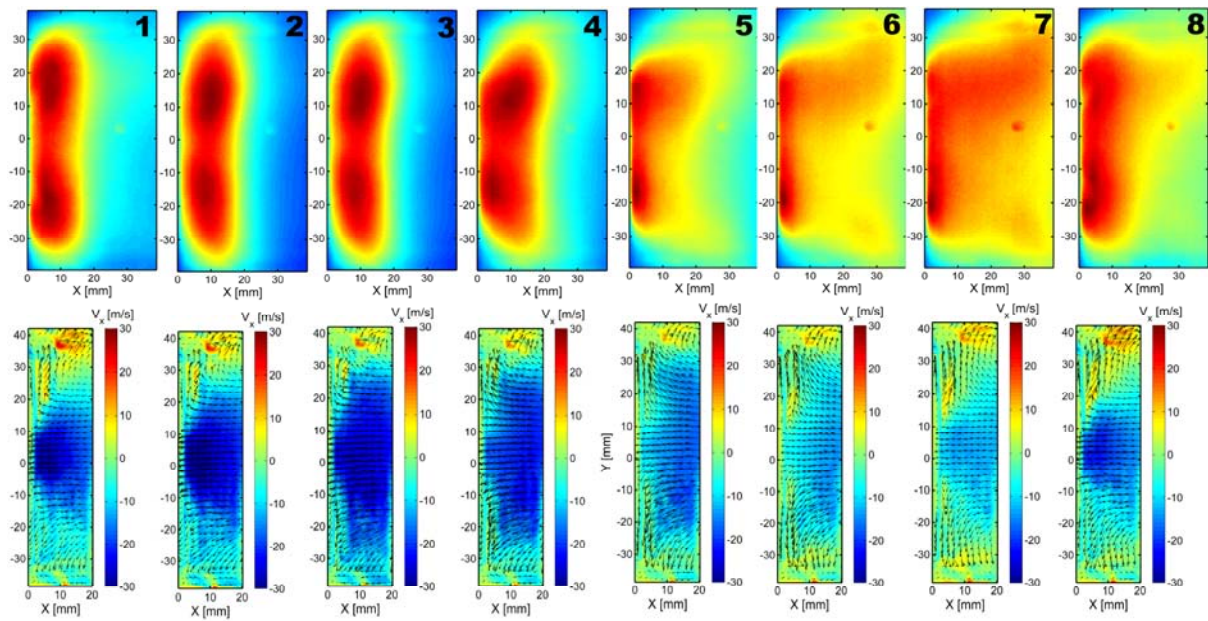
Figure 8 – Phase averaged OH* Chemiluminescence and Axial Velocity.